Ocean & Sea Ice SAF

The EUMETSAT OSI SAF Sea Ice Concentration Algorithm

Algorithm Theoretical Basis Document

Product OSI-401-b

Version 1.5

April 2016

Rasmus Tonboe and John Lavelle

Documentation Change Record

Document version	Software version	Date	Change	Description
v 1.0	v 1.0	10/12/11		First version.
V 1.1		20/06/12	minor	After review
V 1.2		19/12/13	minor	Description of uncertainty model
V 1.3		10/04/15	minor	Description of level 3 processing
V 1.4		22/07/15	minor	Description of land spillover correction
V 1.5		29/04/16	minor	Change Instrument F17 to F18

The software version number gives the corresponding version of the OSI SAF High Latitude software chain which was used to produce the reprocessing data set.

CONTENTS

1. Introduction

1.1 OSI SAF overview

The Ocean and Sea Ice Satellite Application Facility, OSI SAF, is a EUMETSAT project that started in 1997. The OSI SAF is a part of the EUMETSAT distributed ground segment for production of operational near real time value added satellite products. The OSI SAF delivers a range of air-sea interface products, namely: sea ice characteristics, SST, radiative fluxes and wind over open water. The sea ice products are sea ice concentration, the sea ice emissivity and temperature, sea ice edge, sea ice type and sea ice drift.

The OSI SAF project is managed by CMS, Meteo-France. The sea ice products are produced at the OSI SAF High Latitude processing facility under the responsibility of the Norwegian Meteorological Institute, operated jointly by the Norwegian and Danish Meteorological Institutes.

1.2 Sea ice concentration algorithm

Since the start of the operational production of sea ice products in 2002 the growing user group has brought more focus on expanding the available data set. It was therefore decided to reprocess historical passive microwave data to extend the OSI SAF sea ice data set. This effort was started in 2006 as a part time EUMETSAT visiting scientist activity in collaboration with the UK Met Office. The goal was to reprocess the SSM/I data record. A collaboration was also established with NSIDC to include the SMMR data record in the project, and an EUMETSAT visiting scientist project was set up for this task. The OSI SAF project team and these two Visiting Scientist projects initiated the OSI SAF re-processing and produced a first version of the dataset based on the SSM/I data. Later further improvements have been implemented before the current version was finished. The intension with the reprocessing project was also to further develop and update the sea ice concentration algorithm which is used for the day to day processing. This ATBD describes the first step towards unifying the day to day and the reprocessing sea ice concentration algorithms. Compared to the old day to day algorithm this new algorithm adjusts to the actual water and ice signatures and ensures inter-sensor calibration.

This product fulfills the requirement OSI-PRD-PRO-205 in the OSI SAF Product Requirement Document [RD.1]. No data or validation results are presented in this document. The data are presented in the product users manual [RD.2]. The validation results of the methodology are presented in the validation report [RD.3].

1.3 Ownership and copyright of data

The OSI SAF sea ice concentration data has been produced under responsibility of Norwegian Meteorological Institute and Danish Meteorological Institutes. The ownership and copyrights of the data set belongs to EUMETSAT. The data set is distributed free of charge, but EUMETSAT must be acknowledged when using the data. EUMETSAT's copyright credit must be shown by displaying the words "copyright (year) EUMETSAT" on each of the products used. The user registration ensures that all users are informed about potential updates or processing anomalies and the feedback from users is important argumentation for the project team when defining new development activities. We urge anyone to use the data and provide feedback to the project team.

1.4 Acknowledgment

1.5 Glossary

AMSR	Advanced Microwave Scanning Radiometer
ATBD	Algorithm Theoretical Basis Doccument
CMS	Centre de Météorologie Spatiale
CDOP	Continuous Development and Operations Phase (OSI SAF project)
DMI	Danish Meteorological Institute
DMSP	Defense Meteorological Satellite Program
ECMWF	European Centre for Medium range Weather Forecast
FTP	File Transfer Protocol
EUMETSAT	European Organization for the Exploitation of Meteorological Satellites
met.no	Norwegian Meteorological Institute
NASA	National Aeronautics and Space Administration
NSIDC	National Snow and Ice Data Center
NWP	Numerical Weather Prediction
OSI SAF	Ocean and Sea Ice Satellite Application Facility
RTM	Radiative Transfer Model
SAR	Synthetic Aperture Radar
SSM/I	Special Sensor Microwave/Imager
SSMIS	Special Sensor Microwave Imager Sounder
SMMR	Scanning Multi-channel Microwave Radiometer

1.6 Reference Documents

[RD.1] OSI SAF CDOP2 Product Requirement Document, v2.5.

[RD.2] OSI SAF Sea Ice Concentration Product Users Manual, v1.0

[RD.3] OSI SAF Sea Ice Concentration Reprocessing Product Validation Report, v1.1.

2. Process Overview

Figure 1 shows the processing flow chart for the level 2 and 3 production.

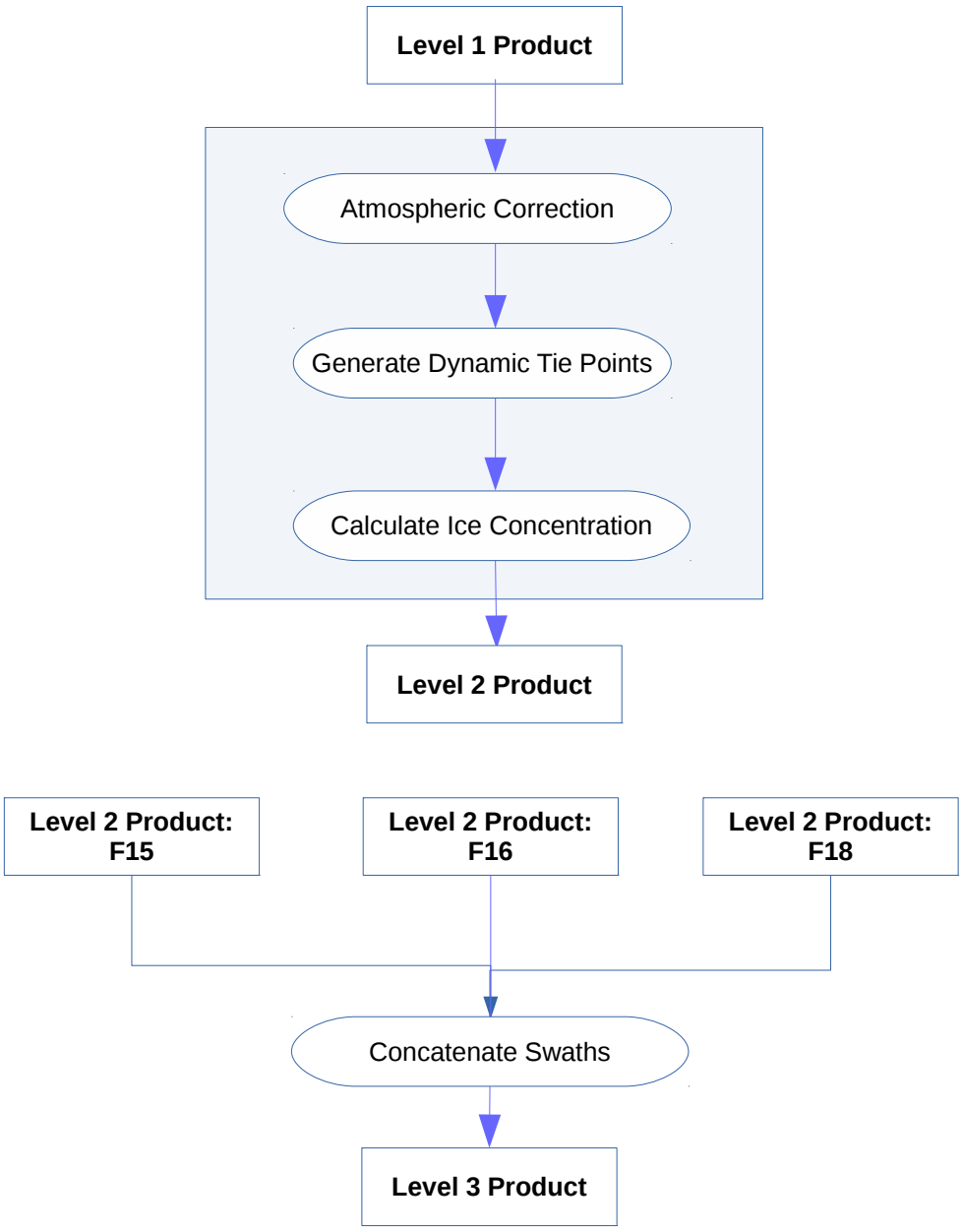

Figure 1: Flow diagram for the level 2 and 3 products

In the first step, as Radiative Transfer Model (RTM) is applied for the atmospheric correction as described in Section 3.2. In the second step the dynamic tie points are generated, as described in Section 4.3. In the third step ice concentration algorithm is applied, as described in Section 4.1. The steps are applied to each satellite: F15, F16 and F18. Finally, for the level 3 product, the swaths from each are concatenated as described in Section 4.5.

3. Input data

This chapter describes the SSMIS satellite data which can be processed by the OSI SAF sea ice concentration algorithm. In fact the algorithm is flexible and it can process other types of microwave radiometer data such as SSM/I, SMMR, and AMSR. Further, the algorithm is using numerical weather prediction (NWP) data for correction of the brightness temperatures prior to calculating the sea ice concentration. The NWP parameter fields are briefly described.

3.1 The SSMIS constant incidence angle scanning microwave radiometer satellite data

The SSMIS is a polar orbiting conically scanning radiometer with constant incidence angle around 50deg and a swath width of about 1700km. It has window channels near 19, 37, 91, and 150GHz and sounding channels near 22, 50, 60, and 183 GHz. The SSMIS temperature sounding channels 1-4 near 50GHz vertical polarization penetrate into the lower troposphere and partially to the surface (Kunkee et al., 2008). The algorithm is using brightness temperature swath data as input. It is using the 19V, the 37V and the 37H channel data.

3.2 NWP data and radiative transfer model correction

The brightness temperatures (Tb) are corrected explicitly for wind roughening over open water and water vapor in the atmosphere prior to the calculation of ice concentration. The correction is using a radiative transfer model function (RTM) and NWP data. Over areas with both ice and water the influence of open water roughness on the Tb's and the ice emissivity is scaled linearly with the ice concentration. The emissivity of ice is given by standard tie-point emissivities. The correction procedure is described in detail in Andersen et al. (2006B). The NWP model grid points are co-located with the satellite swath data in time and space and a correction to the Tb's is applied.

The following prognostic variables are taken from the ECMWF operational forecast model output: wind speed, 2m air temperature, total column water, total column liquid water.

The representation of atmospheric liquid water column in the NWP data is not suitable to use for Tb correction (see Andersen et al., 2006B). The Tb's are therefore not corrected for the influence of liquid water. It is constrained to zero in the RTM. The RTM is described in Wentz (1997) and in the next section, Section 4.

4. Algorithms

4.1 The ice concentration algorithm

The two ice concentration algorithms are the Bootstrap algorithm in frequency mode (Comiso, 1986; Comiso et al., 1997), and the Bristol algorithm (Smith, 1996). These two algorithms are used in combination as a hybrid algorithm.

4.1.1 Selection of algorithm

When selecting an ice concentration algorithm it is important to ensure low sensitivity to the error sources, including variability in atmospheric emission and surface emission. It is particularly important to find low sensitivity to the parameters which are not corrected for using auxiliary data, such as cloud liquid water in the atmosphere and for ice surface emissivity variability. For climate time series it is important to find an algorithm using the 19 and 37 GHz channels which can be used as far back in time as possible, including the SMMR period from 1978 to 1987 and the first SSM/I (F8) from 1987 to 1991.

The analysis of atmospheric sensitivity in Andersen et al. (2006B) showed that the Bootstrap frequency mode algorithm (Comiso, 1986) had the lowest sensitivity to atmospheric noise over open water. Furthermore, the comparison to high resolution SAR imagery in Andersen et al. (2007) revealed that among the algorithms using the low frequency channels (19 and 37 GHz), the Bristol algorithm (Smith, 1986) had the lowest sensitivity to ice surface emissivity variability. In addition this algorithm had a low sensitivity to atmospheric emission in particular at high ice concentrations.

Consequently, a hybrid algorithm has been established as a linear combination of two of the tested algorithms, the Bristol algorithm and the Bootstrap frequency mode algorithm. To ensure an optimum performance over both marginal and consolidated ice, and to retain the virtues of each algorithm, the Bristol algorithm is given little weight at low concentrations, while the opposite is the case over high ice concentrations.

4.1.2 The hybrid ice concentration algorithm

The Bootstrap algorithm (Comiso, 1986) is based on the observation of linear clustering of ice Tb's in scatter plots of T_{37v} vs T_{19v} whereas open water Tb's cluster around a single point. It assumes only two surface types: ice and open water, taking into account the variability of both to optimize the detection of small sea ice concentrations. The linear relationship yields the following simple formulation for the total ice concentration, Ct:

$$Ct=(Tb-Tb^{W})/(Tb^{I}+Tb^{W}), \quad (1)$$

where *Tb* is the measured brightness temperature, Tb^{W} is the open water tie-point, and Tb^{I} is the ice tie-point.

The Bristol algorithm (Smith, 1996) is conceptually similar to the Bootstrap algorithm. In a three-dimensional scatter plot spanned by T_{19v}, T_{37v} and T_{37h} the ice Tb's tend to lie in a plane. The only difference to the Bootstrap algorithm is that instead of viewing the data in the T_{19v}, T_{37v} space, the Bristol algorithm views the data perpendicular to the plane in which the data lies, i.e. in a transformed coordinate system:

$$Bristol\_x=T_{37v}+1.045T_{37h}+0.525T_{19v}, \quad (2a)$$

$$Bristol\_y=0.9164T_{19v}-T_{37v}+0.4965T_{37h}. \quad (2b)$$

The remaining analysis is identical to the Bootstrap algorithm.

The Bootstrap algorithm is used over open water and the Bristol algorithm is used over ice. At intermediate concentrations up to 40% the ice concentration is an average weighted linearly between the two algorithms. This hybrid algorithm is the OSI SAF sea ice concentration algorithm.

4.1.3 Tb correction for water vapor and open water surface roughness variability

Using the model function presented in 4.1.4, the Tb's are corrected for the influence of water vapor in the atmosphere and open water surface roughness caused by wind shear. The model function is a semi empirical radiative transfer ocean model describing the Tb as a function of sea surface temperature, surface wind friction velocity, total atmospheric water vapor, total cloud liquid water and surface air temperature. The model function used for SSMIS processing is described in Wentz (1997). The correction procedure is described in Andersen et al. (2006B). At intermediate ice concentrations the surface emission term is a linear combination of ice emissivity derived from tie-point signatures and the open water emissivity derived from the model.

4.1.4 The model function for open water and sea ice

The model function is using the simplified radiative transfer equation for isotropic conditions, which is adequate for many applications including this one, together with regressions describing the sensitivity to atmospheric and surface parameters. The radiative transfer equation for the top of the atmosphere brightness temperature, F:

$$F(W,V,L)=TBU+\tau[E*TS+(1-E)(\Omega*TBD+\tau*TBC)] \quad (3)$$

where V [mm] is the total water vapor, W [m/s] is the wind speed (at 10m) and L [mm] is the total liquid water in the atmospheric profile (here L=0). E is the surface emissivity, TBC [K] is the cosmic background radiation (2.7K), τ is the atmospheric transmittance, TBU [K] and TBD [K] are the up and down welling atmospheric brightness temperatures. TS [K] is the physical surface temperature and Ω is the reflection reduction factor due to wind induced surface roughness. The subscript i indicates each of the channels 19v, 19h, 37v and 37h. If no I is given then the quantity is independent of frequency:

$$\text{For vertical polarization: } \Omega_i=1+2.5*(\sigma_i^2-68*\sigma_i^6)*\tau_i^3 \quad (4a)$$

$$\text{For horizontal polarization: } \Omega_i=1+6.1*(\sigma_i^2-68*\sigma_i^6)*\tau_i^2 \quad (4b)$$

where the sea surface slope variance, σ is:

$$\sigma_i=\text{sqrt}(5.22E\text{-}3*Xi_i*W) \quad (4c)$$

Table 1. Model coefficients and constants.

	19V	**19H**	**37V**	**37H**
c0	240.58E+0	240.58E+0	239.55E+0	239.55E+0
c1	305.96E-2	305.96E-2	248.15E-2	248.15E-2
c2	-764.41E-4	-764.41E-4	-438.59E-4	-438.59E-4
c3	885.95E-6	885.95E-6	278.71E-6	278.71E-6
c4	-40.80E-7	-40.80E-7	-3.23E-7	-3.23E-7
c5	0.60E+0	0.60E+0	0.60E+0	0.60E+0
c6	-0.16E+0	-0.16E+0	-0.57E+0	-0.57E+0
c7	-2.13E-2	-2.13E-2	-2.61E-2	-2.61E-2
a0	11.80E+0	11.80E+0	28.10E+0	28.10E+0
av1	2.23E-3	2.23E-3	1.85E-3	1.85E-3

av2	0.00E-5	0.00E-5	0.17E-5	0.17E-5
ε0	162.53E+0	83.88E+0	186.31E+0	101.42E+0
ε1	-25.70E-2	-52.22E-2	-56.37E-2	-85.88E-2
ε2	17.29E-3	18.76E-3	14.81E-3	20.76E-3
ε3	-11.77E-5	-9.25E-5	-2.96E-5	-7.07E-5
ε4	21.62E-1	-14.72E-1	21.23E-1	-17.01E-1
ε5	0.70E-2	0.21E-2	1.17E-2	0.55E-2
ε6	0.45E-1	-0.16E-1	0.41E-1	-0.19E-1
ε7	0.14E-4	-1.10E-4	-0.71E-4	-1.27E-4
M1	0.46E-3	3.01E-3	-0.09E-3	3.91E-3
M2	3.78E-3	7.50E-3	2.38E-3	7.00E-3
Xi	0.688	0.688	1	1
Eice	0.95	0.90	0.93	0.88

Tvapor is a sea surface temperature which is representative for water vapor in the atmosphere (Eq. 18A in Wentz, 1997), so if the total water vapor column (V) in the atmosphere is less than 48mm then:

$$Tvapor=273.16+0.8337*V-3.029E-5*(V^{3.33}) \quad (5)$$

Equations 22-23 in Wentz (1997) are not included here because scattering by liquid water is neglected.

The water surface emissivity is the sum of two components: a specular Fresnel emissivity, E0, and a wind induced roughness emissivity, Ew. The specular emissivity component is given by (Eq. 25 in Wentz, 1997) for each of the channels i:

$$E0_i=(\varepsilon0_i+\varepsilon1_i*t+\varepsilon2_i*(t^2)+\varepsilon3_i*(t^3)+\varepsilon4_i*q+\varepsilon5_i*t*q+\varepsilon6_i*(q^2)+\varepsilon7_i*(t^2)*q)/Ts \quad (6)$$

where $q=\Theta-51$ and $t=Ts-273.16$.

The wind induced emissivity over open water where W1=7 and W2=12:

$$\text{For } W<=7m/s: \quad Ew_i=M1_i*W \quad (7a)$$

$$\text{For } 7m/s<W<12m/s: \quad Ew_i=M1_i*W+0.5*(M2_i-M1_i)*((W-W1)^2)/(W2-W1) \quad (7b)$$

$$\text{For } W>=12m/s: \quad Ew_i=M2_i*W-0.5*(M2_i-M1_i)*(W2+W1) \quad (7c)$$

The open water emissivity as a combination of the plane surface specular Fresnel reflection and the wind induced roughness emissivity:

$$E_i=E0_i+Ew_i \quad (8)$$

The cosmic background radiation, TBC, is 2.7K. Equation 17a in Wentz (1997) is describing the down-welling brightness temperature due to water vapor in the atmosphere, Td:

$$Td_i=c0_i+c1_i*V+c2_i*(V^2)+c3_i*(V^3)+c4_i*(V^4)+c5_i*(Ts-Tvapor) \quad (9)$$

and the upwelling brightness temperature, Tu:

$$Tu_i=TD_i+c6_i+c7_i*V \quad (10)$$

The coefficients A:

$$A0_i=(a0_i/TD_i)^{1.4} \quad (11a)$$

$$Av_i = av1_i * V + av2_i * (V^2) \quad (11b)$$

The transmitance through the atmosphere along the line of sight, τ:

$$\tau_i = \exp((-1/\cos(\theta)) * (A0_i + Av_i)) \quad (12)$$

and the up-welling atmospheric Tb

$$Tbu_i = Tu_i * (1 - \tau_i) \quad (13)$$

and the down-welling atmospheric Tb

$$Tbd_i = Td_i * (1 - \tau_i) \quad (14)$$

Finally the simplified radiative transfer equation for the brightness temperature from the atmosphere over open water and sea ice covered surfaces:

$$Tb_i = Tbu_i + \tau_i * ((1-Cice) * E_i * Ts + Cice * Eice_i * Ti + (1-Cice) * (1-E_i) * (\Omega_i * Tbd_i + \tau_i * TBC) + Cice * (1-Eice_i) * (Tbd_i + \tau_i * TBC)) \quad (15)$$

where Ti is the ice effective temperature for each channel and Ts is the physical sea surface temperature. Cice is the sea ice concentration where 0 is open water and 1 is 100% ice.

4.2 Land Spillover Correction

A land mask is applied to ice concentration maps; however, due to *land spillover,* erroneous ice concentrations are still observed along the coast. Land spillover is caused by the coupling of microwave radiation from the land during the measurement of the sea pixels. The instruments' field of view covers an area larger than a single pixel (the beam pattern at sea level is approximately Gaussian with a radius of 56 km, for the lowest resolution channel) and the large difference in the emissivity between the land and sea corrupts sea pixels which are close enough for part the instrument's field of view to coincide with land.

A land spillover correction scheme is applied in order to mitigate the problem. The objective of the scheme is to eliminate erroneous and keep valid ice concentration data. The following procedure, modified from the one given in Markus et al. (2009), is applied:

1. The pixels of the polar-sterographic grid are classified with respect to their distance in pixels from the coast. Beside the coast they are labeled *1*, the pixels next furthest out are label *2* and the next furthest out again are labeled *3*. Pixels further away than three pixels are labeled 0.
2. Pixels with classes 1 or 2 are assessed for erroneous sea ice concentrations by analysing the 11 by 11 pixel neighbourhood (equivalent to 10 km). This area encompasses the SSMI antenna's beam pattern. Pixels with values of 3 or 0 will not be changed.
3. In the 11 by 11 pixel neighborhood, if the coastal mask is 1 or 2 and ice concentration is below the theoretical value of land spillover the ice concentration is set to 0.
4. In the 11 by 11 pixel neighborhood, if the coastal mask is 1 or 2 and all type 3 pixels have ice concentration less than 15%, the signal is assumed to be due to noise, and the ice concentration is set to 0.
5. The theoretical concentration caused by land spillover is determined as follows: Calculate an average sea ice concentration for the 11 by 11 pixel box, assuming all the ocean pixels have zero ice concentration and all the land pixels have a concentration of 90%, approximating a theoretical concentration caused by land spillover only.
6. If the SSMI ice concentration is less than or equal to this value, the pixel at centre of box is set to 0.

The coastal correction procedure fails for particular regions, such as the Baltic, where the sea pixels are surrounded by near-by land. In these regions, coastal regions are masked out.

4.3 Dynamical tie-points

Tie-points are typical signatures of 100% ice and open water which are used in the ice concentration algorithms as a reference. The tie-points are derived by selecting Tb's from regions of known open water and 100% ice. Usually these tie-points are static in time and space, but they can be adjusted to follow the seasonally changing signatures of ice and open water. Static tie-points are prone to be affected by sensor drift, inter sensor calibration differences and climatic trends in surface and atmospheric emission. The data must therefore be carefully calibrated before computing the ice concentrations. Here we use dynamic tie-points, a method that minimizes these unwanted effects, with or without prior calibration.

During winter, in the consolidated pack ice well within the ice edge, the ice concentration is very near 100 % (Andersen et al., 2007). This has been established using high resolution SAR data, ship observations and by comparing the estimates from different ice concentration algorithms. The apparent fluctuations in the derived ice concentration in the near 100% ice regime are primarily attributed to snow/ice surface emissivity variability around the tie-point signature and only secondarily to actual ice concentration fluctuations. In the marginal ice zone the atmospheric emission may be significant. The fluctuations due to atmospheric and surface emission are systematic. In fact, different algorithms with different sensitivity to atmospheric and surface emission compute very different trends in sea ice area on seasonal and decadal time scales (Andersen et al., 2007). This means that not only do the sea ice area have a climatic trend, but the atmospheric and surface constituents affecting the microwave emission are also changing. For example, different wind patterns, water vapor and liquid water concentrations in the atmosphere, snow depth, fraction of perennial ice etc. In an attempt to compensate for the influence of these unwanted trends the tie-points are derived dynamically using a mean of the last 30 days of swath data. It is assumed that ice concentrations from the NASA Team algorithm above 95 % are in fact near 100 % ice and that the mean value of these data points can be used to derive the ice tie-point. The NASA Team ice concentration is the initial guess before the iteration and the OSI SAF ice concentration does not depend on the NASA Team ice concentration. The analysis of SAR data in Andersen et al. (2007) from the central arctic showed that during winter there is more than 99% ice cover. During strong ice drift divergence and during the summer there may situations where this is not the case. However, during one month of tie-point data collection we are sure to have captured the situations with near 100% ice cover. The standard deviation of the tie-point is included in the total ice concentration error estimate which is the justification for this assumption.

Regions of open water are selected near the ice edge using the monthly NSIDC maximum ice extent climatology plus additional 100 km. There is no attempt to compensate explicitly for sensor drift or inter-sensor calibration differences between the seven different sensors used in the analysis. The dynamical tie-point method is in principle compensating for these problems in a consistent manner.

Dynamical tie-point algorithm summary:

1.For each swath grid point the NASA team ice concentration (static tie-points, Comiso et al. 1997) is added.

2.The atmospheric correction is applied based on the NASA Team concentration and the NWP data.

3.The dynamical tie-points are computed using the swath data for one day i.e. the number of data points for the ice and the water tie-points, the coordinates for the ice line and for the the water point. Dynamical tiepoints are computed separately for the Bootstrap algorithm and the Bristol algorithm and both sets are used by the OSI SAF hybrid algorithm.

4.The daily tie-point coordinates are combined into a 30day running mean tie-point which is used in the further processing.

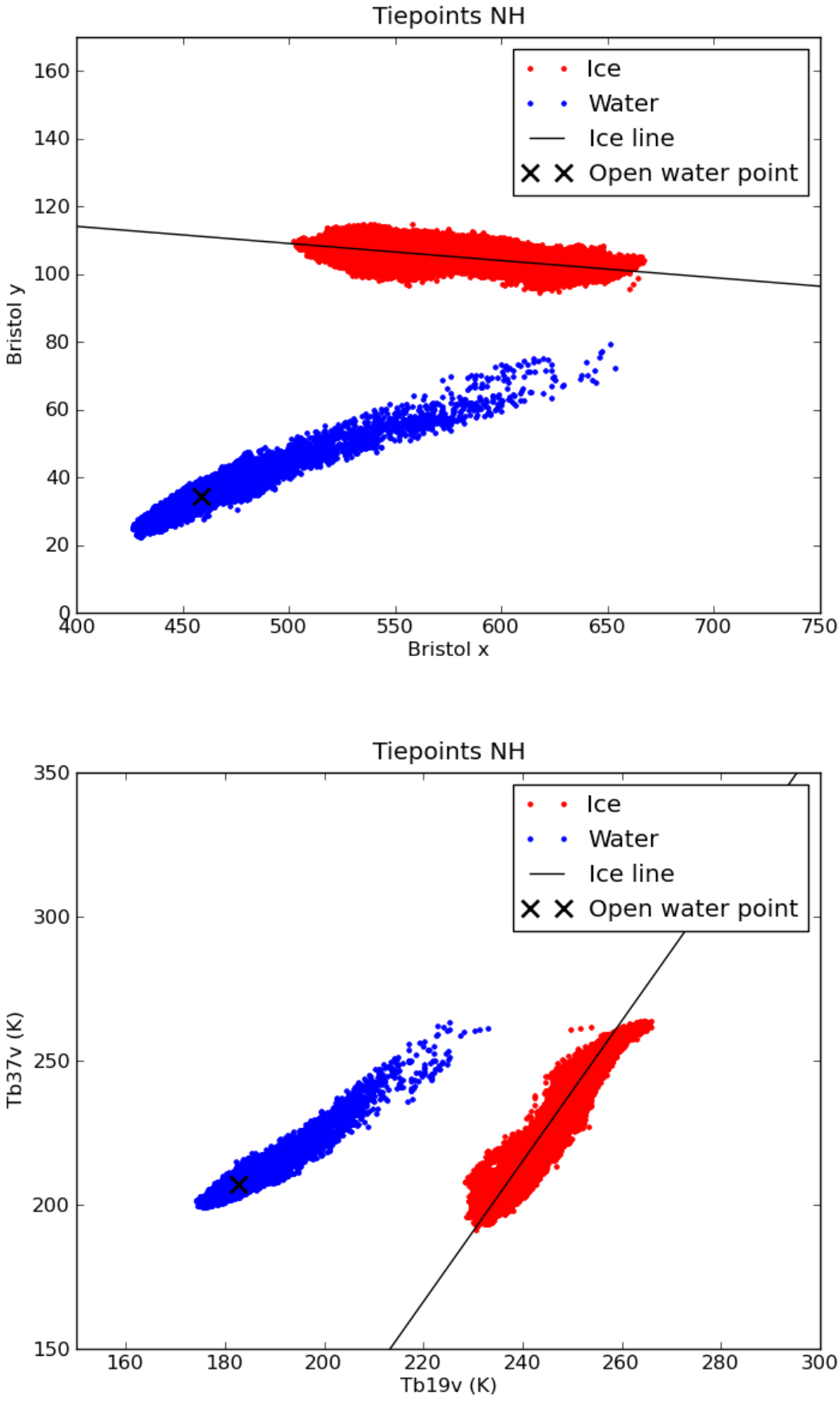

Figure 3: The Comiso boot-strap dynamical tie-point for one day, northern hemisphere

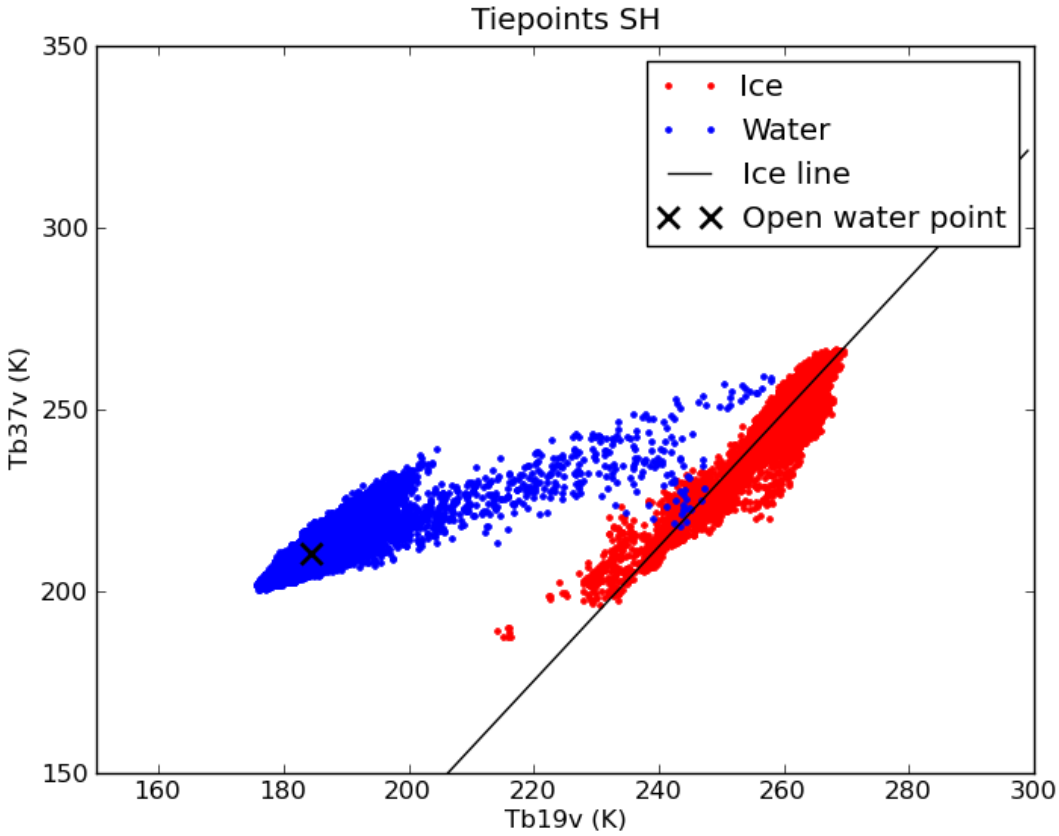

Figure 4: The Comiso boot-strap dynamical tie-point one day, southern hemisphere

4.4 Sea ice concentration uncertainties

Uncertainty estimates are needed when the ice concentration data are compared to other data sets or when the ice concentrations are assimilated into numerical models. The mean accuracy of some of the more common algorithms, used to compute ice concentration from SSM/I data, such as NASA Team and Bootstrap are reported to be 1-6 % in winter (Andersen et al., 2006A). This is also achieved with the OSISAF algorithm.

The polar atmosphere is generally transparent for microwave radiation in between the sounding channels called the atmospheric windows near 19, 37, 91, and 150 GHz. For typical polar atmospheric states the down-welling emission at the surface is about 5-15 K at 18 GHz, 20-40 K at 36 GHz, 30-100 K at 90 GHz. For comparison, the sea ice surface emission is typically 150-260 K. When computing the ice concentration using the atmospheric window channels, the atmospheric emission and scattering is an error source. The tie-points are typical ice and water signatures representative on a hemispheric scale. Deviations from the typical surface emission signatures result in ice concentration uncertainties. The SSMIS instrument has large foot-prints on the ground, and the algorithms with the lowest sensitivity to both atmospheric and surface emissivity variability use Tb's at different frequencies with different foot-print size. Representing these large foot-prints on a finer, predefined grid results in a representativeness error. In addition there is the geo-location error, sensor noise, drift, and sea ice variability over the sampling period.

4.4.1 Algorithm and tie-point uncertainties

Both the water surface and ice surface emissivity variabilities result in ice concentration uncertainties. Emission and scattering in the atmosphere also affects the Tb's and the computed ice concentrations. Different algorithms have different sensitivities to these surface and atmospheric parameters (Andersen et al., 2006B). Further, both the atmospheric and surface parameters affecting the ice concentration estimates have climatic trends (Andersen et al., 2007). To minimize the uncertainties due to these two parameters, the Tb's are corrected using NWP data for atmospheric humidity and open water roughness in this reanalysis. The dynamical tie-points minimizes uncertainty due to the climatic trends in the atmosphere and on the ice surface on a hemispheric scale while regional trends may still exist.

4.4.2 Representativeness error

Foot-print sizes for the channels used for ice concentration mapping range from about 56 km for the 19 GHz channels to about 33 km for the 37 GHz channels. Foot-prints of uneven size are combined in the algorithms when computing the ice concentration. The foot-print ice concentration is represented on a predefined grid. The ice concentration data are normally represented on a finer grid (typically 10 or 25 km) than the sensor resolution (33 to 56 km). This is sometimes called smearing. The combination of foot-prints of uneven size in the ice concentration algorithm results in an additional smearing effect. This we call the foot-print mismatch error. The smearing and the foot-print mismatch error can not be estimated separately. However, the combined error can be estimated if all other error sources and the ice cover reference are known *a priori*. It can also be simulated using high resolution ice concentration reference data and a model for the satellite measurement foot-print patterns.

4.4.3 Geo-location error

A geo-location error occurs when the satellite is not exactly oriented. Simulations show that because the foot-prints are large compared to the typical geo-location errors (about 5km), the geo-location error is small. In addition there is the temporal differences between each pair of Tb observation.

4.4.4 The sea ice concentration uncertainty algorithm

The representativeness error is computed as a function of ice concentration using a model. The other error sources are computed using the hemispheric standard deviation of the measurements over open water and over near 100% ice respectively. The ice concentration algorithm provide ice concentrations which are greater than 100% and less than 0%. These unphysical concentrations are truncated in the processing. Therefore we write the ice concentration, ic:

$$ic = (1 - A(ic))\,water + A(ic)\,ice \qquad (16),$$

where ic is the ice concentration calculated by the algorithm and A is the truncated ice concentration as a function of the algorithm ice concentration ic is:

$$A(ic) = \prod(ic)\,ic + H(ic - 1) \qquad (17),$$

where $\prod(x)$ is the Boxcar function and H(x) the Heaviside step function.

if ic≤0 then A=0

if 0<ic<1 then A=ic (18)

if ic≥1 then A=1

Using equation 16 and assuming the uncertainty for the ice and water part is independent this leads to a total tie-point uncertainty i.e

$$e_{tie-point}(A(ic)) = \sqrt{(1-A(ic))^{2}_{water}{}^{2} + A^{2}(ic)\,e^{2}_{ice}} \qquad (19)$$

where

$$e_{water} = e(IC(P_{water})) \qquad (20),$$

and open water is determined by a monthly varying ocean mask, IC is the functional mapping of the ice concentration algorithm and Pc denotes the set of swath pixels for all swaths (used for calculating the daily product) selected on the condition C. The condition C is either ice or water.

$$e_{ice} = e(IC(P_{NT>0.95})) \qquad (21),$$

is the STD of the ice concentrations where the NASA team (NT) algorithm finds ice concentrations greater than 0.95.

4.5 Level 3 processing

The sea ice concentration and corresponding uncertainties are computed on the swath files.

The swath files for one day are then concatenated and resampled onto the OSISAF grid. using the *pyresample* python library The *resample_gauss* function is used to resample, using a Gaussian weighting.

$$\exp(x^2/\sigma) \qquad (22),$$

A radius_of_influence of 75 km is used and the gauss resampling is calculated from 3 dB FOV levels.

Uncertainty estimates in the form of weighted standard deviation are be obtained also from this function. The principle, used to calculate the uncertainty, is to consider the resampled values as a weighted average of values sampled from a statistical variable. An estimate of the standard deviation of the distribution is calculated using the unbiased weighted estimator given as:

$$std = \sqrt{(V_1/(V_1^2+V_2))\sum_i w_i (x_i - r)^2} \qquad (23),$$

where r result is the result of the resampling, x_i is the value of a contributing neighbour and w_i is the corresponding weight. The coefficients are given as $V_1 = \sum_i w_i$ and $V_2 = \sum_i w_i^2$. The standard deviation is only calculated for elements in the result where more than one neighbour has contributed to the weighting.

The procedure is described in the product user manual.

5. References

Andersen, S., L. Toudal Pedersen, G. Heygster, R. Tonboe, and L Kaleschke, Intercomparison of passive microwave sea ice concentration retrievals over the high concentration Arctic sea ice. *Journal of Geophysical Research* 112, C08004, doi10.1029/2006JC003543, 2007.

Andersen, S., R. T. Tonboe and L. Kaleschke. Satellite thermal microwave sea ice concentration algorithm comparison. *Arctic Sea Ice Thickness: Past, Present and Future*, edited by Wadhams and Amanatidis. Climate Change and Natural Hazards Series 10, EUR 22416, 2006A.

Andersen, S., R. Tonboe, S. Kern, and H. Schyberg. Improved retrieval of sea ice total concentration from spaceborne passive microwave observations using Numerical Weather Prediction model fields: An intercomparison of nine algorithms. *Remote Sensing of Environment104, 374-392*, 2006B.

Comiso J.C, D.J. Cavalieri, C.L. Parkinson, and P. Gloersen. Passive microwave algorithms for sea ice concentration: A comparison of two techniques. *Remote Sensing of Environment* 60, 357-384, 1997.

Comiso J.C. Characteristics of arctic winter sea ice from satellite multispectral microwave observations. *Journal of Geophysical Research* 91(C1), 975-994, 1986.

Kunkee, D. B., G. A. Poe, D. J. Boucher, S. D. Swadley, Y. Hong, J. E. Wessel, and E. A. Uliana, 2008. Design and evaluation of the first special sensor microwave imager/sounder, IEEE Trans. Geo. Rem. Sens. 46(4), 863-883.

Markus T, Cavalieri D. The AMSR-E NT2 Sea Ice Concentration Algorithm: its Basis and Implementation. *Journal of The Remote Sensing Society of Japan*. 2009; 29 (1):216-225.

Smith, D. M. Extraction of winter total sea ice concentration in the Greenland and Barents Seas from SSM/I data. *International Journal of Remote Sensing 17*(13), 2625-2646, 1996.

Wentz, F. J. A well-calibrated ocean algorithm for SSM/I. *Journal of Geophysical Research* 102(C4), 8703-8718, 1997.